Electronic Supplementary Material (ESI) for Nanoscale.
This journal is © The Royal Society of Chemistry 2016

Supplementary Information

for

Thermal conductivity of individual silicon nanoribbons

Lin Yang,[1,†] Yang Yang,[1,†] Qian Zhang,[1,†] Yin Zhang,[1,3] Youfei Jiang,[2] Zhe Guan,[2] Matthew Gerboth,[1] Juekuan Yang,[3] Yunfei Chen,[3] D. Greg Walker,[1] Terry T. Xu,[2] and Deyu Li[1,]*

[1]Department of Mechanical Engineering, Vanderbilt University, Nashville, TN 37235, USA

[2]Department of Mechanical Engineering and Engineering Science, The University of North Carolina at Charlotte, Charlotte, NC 28223, USA

[3]School of Mechanical Engineering and Jiangsu Key Laboratory for Design and Manufacture of Micro-Nano Biomedical Instruments, Southeast University, Nanjing, 210096, P. R. China

†: These authors contributed equally to this work

*: Author to whom correspondence should be addressed. E-mail: deyu.li@vanderbilt.edu

1. Si nanoribbon fabrication

The nanoribbon fabrication started with 6″ (150 mm) diameter SOI wafers (p-type boron doped Si (100) with a dopant density of $0.7{-}1.5\times10^{15}$ cm^{-3}, Simgui Technology Co., Ltd.) with a 140 nm thick top silicon device layer and a 500 nm buried oxide (BOX) layer. In the fabrication process, the SOI wafer first went through a timed dry oxidation process to oxidize a targeted thickness of the device silicon layer, after which the resulted silicon oxide layer was removed with buffered oxide etch (BOE 6:1). The thickness of the remaining silicon device layer was measured with an ellipsometry method. Then the wafer was cut into 30×30 mm pieces and patterned into nanoribbons using E-beam lithography (JEOL 6300) and reactive ion plasma etching (PlasmaTherm 770), leading to ribbons anchored on two separated islands. Finally, wet hydrofluoric acid (HF) etching (10:1) and critical point dry was used to remove the underneath BOX and release the Si nanoribbons into freestanding structures.

2. The effects of the inner radiation shield

The effects of the inner radiation shield mounted on the sample holder were tested with thermal conductivity measurements on the same silicon nanoribbon sample with and without the inner radiation shield. The measured electrical resistance of the heating and sensing membrane is very close for these two different configurations at low temperatures. However, without the inner radiation shield, as temperature increases, radiation heat transfer from the device to the environment becomes non-trivial, causing the temperature of the Pt thermometer to be lower than the setting temperature of the heating stage. This leads to a 4.2% and 3.7% difference of the measured resistance at 420 K for the heating and sensing membranes, respectively, compared with the case that has the inner radiation shield mounted. This seemingly small difference, however, renders an error in the derived temperature coefficient of resistance (TCR), and eventually an error in the derived temperature rise for the heating and sensing membranes.[1,2] The overall effects on the measured thermal conductance is shown in Fig. S1, where the measured sample thermal conductance for the case with double radiation shields starts to be higher than that for a single radiation shield at 150 K. The difference increases as the temperature ramps up and eventually results in a 23% difference in the measured sample thermal conductance at 420 K with a higher value for the double radiation shield case. Importantly, the temperature dependence is also quite different at higher temperature, which renders a great challenge in modeling the thermal conductivity. In fact, we cannot obtain a good fitting for the experimental data obtained without the inner radiation shield.

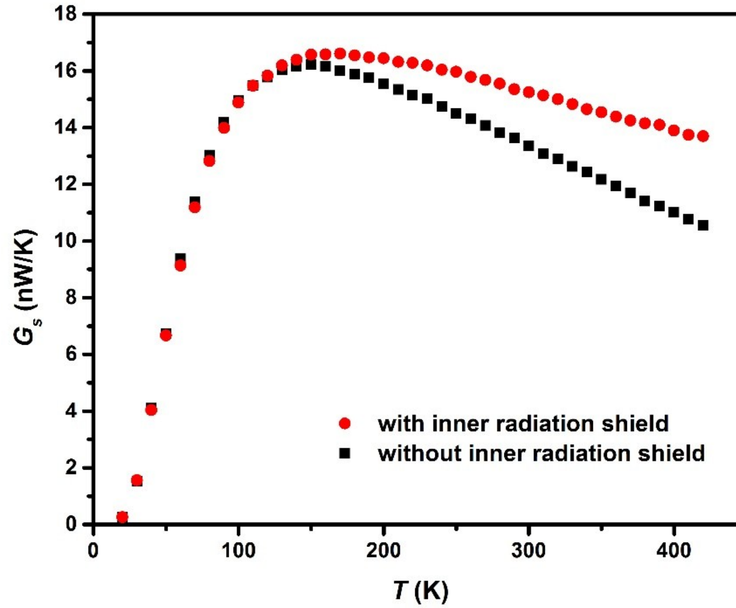

Figure S1. Comparison of measured sample thermal conductance of a 33 nm thick, 138 nm wide Si nanoribbon with and without the inner radiation shield.

3. Oxide thickness

In order to determine the thickness of the amorphous oxide layer at the surface of the Si nanoribbons, we applied hydrofluoric acid etching on a double Si nanoribbon stack, and then transfer this nanoribbon bundle to a flat silicon chip for atomic force microscopy (AFM) cross-section measurement, as shown in Fig. S2a. We have experimentally determined that after storing the etched double ribbons in a high vacuum ($<10^{-6}$ mbar) chamber, the interface between the two ribbons is free of oxide afterwards. Therefore, native oxide only exists at the top and bottom surface. By measuring the thickness of single and double nanoribbon segment (Fig. S2b), and using the relation that 1 nm thick silicon could lead to 2.17 nm oxide,[3] we determined the oxide thickness as ~1.5 nm.

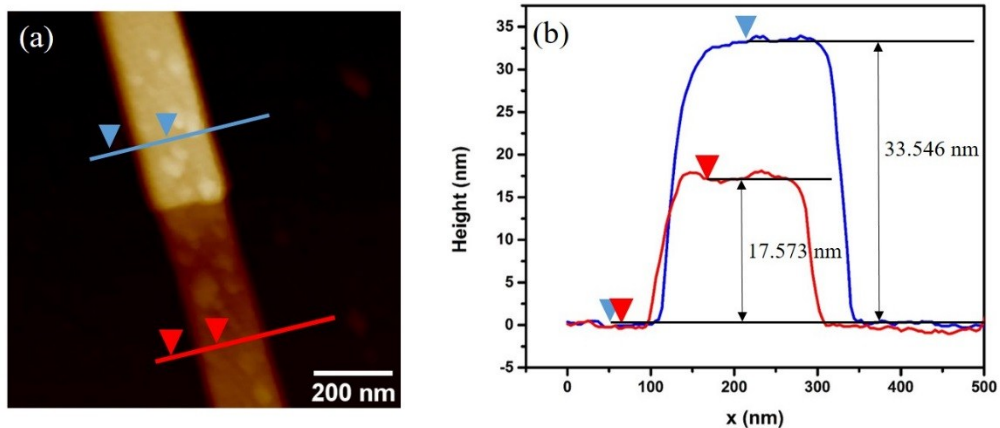

Figure S2. (a) AFM image of a double Si nanoribbon stack. (b) Corresponding thickness at the selected points of single and double ribbon segments.

4. Young's modulus measurement

To measure the Young's modulus, the Si nanoribbon was transferred to a trench of 7 μm wide etched on a silicon chip. A layer of Pt is locally deposited at the two ends of the ribbon through electron beam induced deposition to clamp the ribbon to the substrate. We then measure the deflection of the ribbon with an AFM (Bruker Dimension Icon). Before each measurement, the sensitivity of the cantilever is calibrated by tapping it on the hard Si substrate and the spring constant is extracted through a thermal tune process.

By scanning the Si nanoribbon using AFM, we can locate its middle point across the trench. We then perform the bending test by pushing the middle point to obtain a force-deflection (FD) curve, as shown in Fig. S3. The bending tests were repeated three times for each sample with reproducible results. The Young's modulus of the sample was then extracted through fitting the FD curve using a theoretical model of a suspended elastic string with fixed ends.[4,5] In order to consider the oxide shell effects, we applied the core-shell composite model to obtain the intrinsic Si core Young's modulus,[4,6] shown as fitted curves in Fig. S3. The measured Young's moduli of the nanoribbons are given in Fig. 7 in the main manuscript, which shows a clear dependence on the surface to volume ratio. Importantly, for the thicker ribbons of larger widths, their Young's moduli is close to the bulk value of E_{110} =170 GPa.[4,7] The detailed dimensions of the measured ribbons and extracted Young's modulus for each sample are also listed in Table S1.

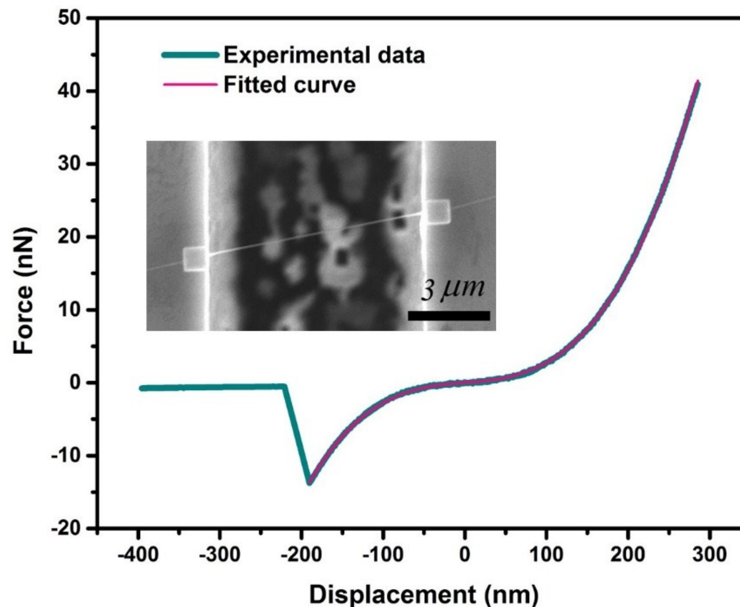

Figure S3. Measured F-D curve (blue) and fitted curve (red) according to the analytical model for a measured Si nanoribbon of 34 nm high, 32 nm wide with a suspended length of 8.4 μm. The extracted Young's modulus is 133 GPa. Inset shows the measured nanoribbon sample suspended over a 7 μm wide Si trench with both ends clamped by a layer of Pt through EBID.

Thick group			
Thickness (nm)	Width (nm)	*S/V* (nm^{-1})	E (GPa)
31	207	0.074	178.3
33	72	0.088	172.2
30	49	0.107	168.9
30	31	0.131	138.9
32	29	0.131	133
Thin group			
19	137	0.120	151.5
19	100	0.125	139.8
19	105	0.124	142.9
19	68	0.135	131
19	64	0.137	125.3
19	68	0.135	119.1
20	45	0.144	106.4

Table S1. Summary of the Si nanoribbons' dimensions for three-point bending test, the corresponding surface-area-to-volume ratio and the measured Young's modulus.

5. Effects of the defect scattering term on the modeled thermal conductivity

The main purpose of the modeling is to show that while we can match the experimental data of thicker ribbons well, the prediction based on the same parameters other than the ribbon dimension cannot fit the results for thinner ribbons. As such, we adopted the best fitting parameters we can get without sticking to the more commonly adopted values.

Previously reported values for the defect scattering parameter in modeling the thermal conductivity of various silicon structures span a large range of 1.32 ~ 70×10^{-45} s^3.[8–13] The most commonly used value of the defect scattering parameter for VLS Si nanowires and thin silicon films is 1.32×10^{-45} s^3, which is analytically determined from isotope concentration.[8] For low and moderately boron doped silicon (boron concentration 3.1×10^{18} and 2×10^{19} cm^{-3}), the adopted defect scattering parameter in literature are 2.4×10^{-45} s^3 and 4×10^{-45} s^3,[13] which are higher than the widely adopted value of 1.32×10^{-45} s^3.

For the silicon nanoribbons in this work, the ribbon is made from lightly boron doped wafers (doping concentration: $0.7–1.5\times10^{15}$ cm^{-3}), which experience the process of thermal oxidation, wet etching and RIE etching. These processes might induce additional defects in the ribbon and as such, we allowed for the defect scattering parameter to be adjustable instead of adopting the value of 1.32×10^{-45} s^3.

In order to test the modeled results for the commonly used value for defects scattering term as $D = 1.32\times10^{-45}$ s^3,[8] we compared it with our best fitting result in Fig. S4. To get the best fitting results for $D = 1.32\times10^{-45}$ s^3, we increased the surface roughness η to 0.21 nm. From Fig. S4, we can see that even though the performance of the best fitting result for $D = 1.32\times10^{-45}$ s^3 is comparable to that of $D = 3.5\times10^{-45}$ s^3 in the high temperature range, the latter one matches much better for low temperature data. As such, we adopted the best fitting results in the main manuscript. Importantly, shown as in Fig. S5, no matter which set of parameters we adopt to achieve

reasonable fitting for the thick group ribbons, the model fails to yield satisfactory fitting for thinner ribbons by simply reducing the ribbon dimensions in the calculation.

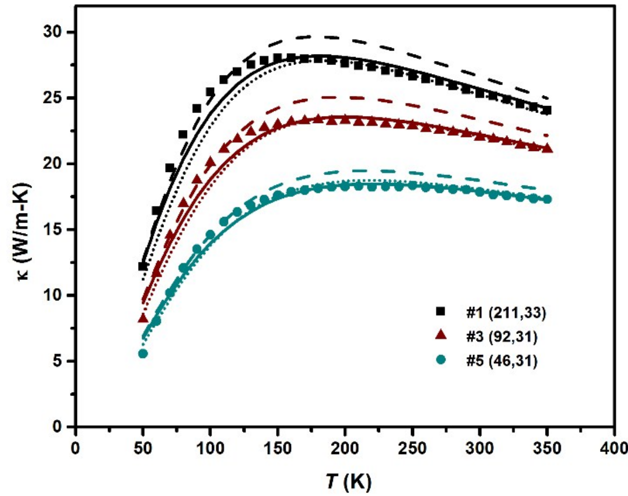

Figure S4. Comparison between measured thermal conductivity and fitted results for three thick group Si nanoribbons with different cross-section dimensions. Solid curves represent the fitted results for D = 3.5×10^{-45} s^3 and η = 0.18 nm, dashed lines are fitted results for D = 1.32×10^{-45} s^3 and η = 0.18 nm, and dotted lines are results for D = 1.32×10^{-45} s^3 and η = 0.21 nm.

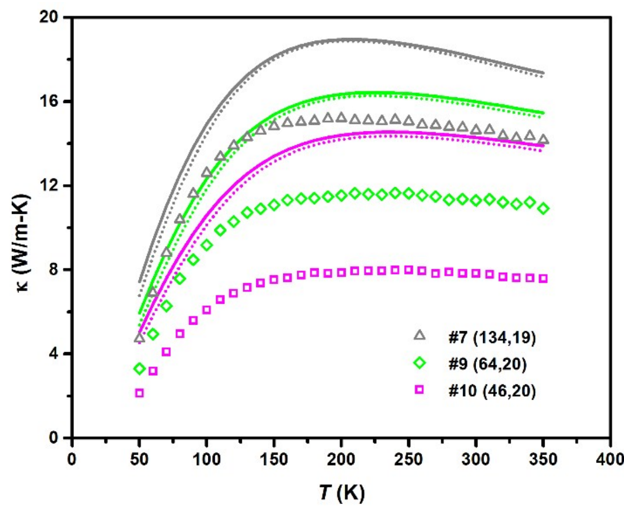

Figure S5. Comparison between measured thermal conductivity and fitted results for three thin group Si nanoribbons with different dimensions. Solid curves represent the fitted results for D = 3.5×10^{-45} s^3 and η = 0.18 nm, while dotted lines are results for D = 1.32×10^{-45} s^3 and η = 0.21 nm.

6. Modeled thermal conductivity for thin group Si nanoribbons considering the elastic softening effects

The deviation of the modeling results for thinner ribbons is to show that without taking into account the elastic softening effects on phonon transport, we cannot obtain satisfactory prediction for the thin group ribbons. In order to consider the elastic softening effects, we further modified the model by scaling down the phonon group velocity using the measured reduced Young's modulus (E) for the thin group Si nanoribbons. As the speed of sound v is related to Young's modulus as $v = \sqrt{E/\rho}$, where ρ is the density, we use a scaling factor for the phonon group velocity as $\sqrt{E_{SiNR}/E_{bulk}}$. As shown Fig. S6, after scaling the phonon group velocity and keeping all other fitting parameters unchanged, the modeled thermal conductivity for thin group Si nanoribbons are much closer to the measured data. In fact, the maximum overestimation of the modeled result for the 20 nm thick and 46 nm wide sample decreases from 83% to 19%. The remaining difference could be due to the simple scaling approach, as the speed of sound doesn't depend on frequency, while phonon group velocity changes remarkably versus phonon frequency. As such, for higher frequency phonons, the scaling factor might not be very accurate.

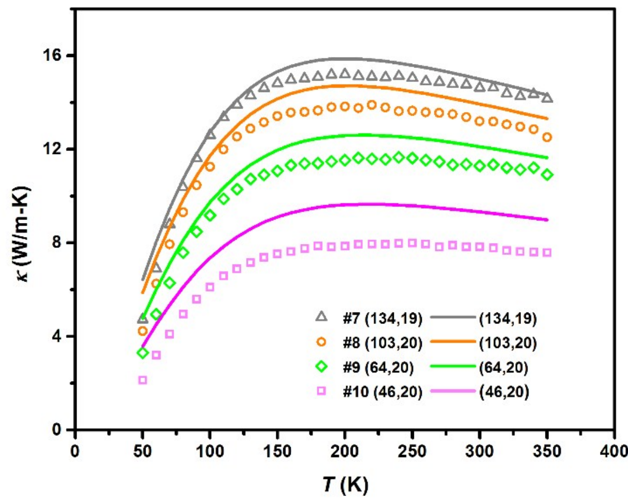

Figure S6. The comparison of measured thermal conductivity and modeled results after considering the elastic softening effects for thin group Si nanoribbons.

References

1. A. L. Moore and L. Shi, *Meas. Sci. Technol.*, 2010, **22**, 15103.
2. L. Shi, D. Li, C. Yu, W. Jang, D. Kim, Z. Yao, P. Kim and A. Majumdar, *J. Heat Transfer*, 2003, **125**, 881.
3. B. E. Deal and A. S. Grove, *J. Appl. Phys.*, 1965, **36**, 3770–3778.
4. Y. Calahorra, O. Shtempluck, V. Kotchetkov and Y. E. Yaish, *Nano Lett.*, 2015, **15**, 2945–2950.
5. L. M. Bellan, J. Kameoka and H. G. Craighead, *Nanotechnology*, 2005, **16**, 1095–1099.
6. C. Q. Chen, Y. Shi, Y. S. Zhang, J. Zhu and Y. J. Yan, *Phys. Rev. Lett.*, 2006, **96**, 1–4.
7. Y. Zhu, F. Xu, Q. Qin, W. Y. Fung and W. Lu, *Nano Lett.*, 2009, **9**, 3934–3939.
8. N. Mingo, *Phys. Rev. B*, 2003, **68**, 113308.
9. W. Liu and M. Asheghi, *J. Appl. Phys.*, 2005, **98**.
10. M. Maldovan, *J. Appl. Phys.*, 2012, **111**, 11–17.
11. N. K. Ravichandran and A. J. Minnich, *Phys. Rev. B*, 2014, **89**, 205432.
12. J.-K. Yu, S. Mitrovic, D. Tham, J. Varghese and J. R. Heath, *Nat. Nanotechnol.*, 2010, **5**, 718–721.
13. J. Lim, H.-T. Wang, J. Tang, S. C. Andrews, H. So, J. Lee, D. H. Lee, T. P. Russell and P. Yang, *ACS Nano*, 2015.